NANO EXPRESS

Open Access

CrossMark

Sensitive and Selective Detection of HIV-1 RRE RNA Using Vertical Silicon Nanowire Electrode Array

Jaehyung Lee[1†], Min-Ho Hong[1†], Sanghun Han[1], Jukwan Na[1], Ilsoo Kim[1], Yong-Joon Kwon[2], Yong-beom Lim[1*] and Heon-Jin Choi[1*]

Abstract

In this study, HIV-1 Rev response element (RRE) RNA was detected via an Au-coated vertical silicon nanowire electrode array (VSNEA). The VSNEA was fabricated by combining bottom-up and top-down approaches and then immobilized by artificial peptides for the recognition of HIV-1 RRE. Differential pulse voltammetry (DPV) analysis was used to measure the electrochemical response of the peptide-immobilized VSNEA to the concentration and types of HIV-1 RRE RNA. DPV peaks showed linearity to the concentration of RNA with a detection limit down to 1.513 fM. It also showed the clear different peaks to the mutated HIV-1 RRE RNA. The high sensitivity and selectivity of VSNEA for the detection of HIV-1 RRE RNA may be attributed to the high surface-to-volume ratio and total overlap diffusion mode of ions of the one-dimensional nanowire electrodes.

Keywords: Nanoelectrode, Silicon nanowire, HIV-1 RRE RNA, Biomolecule sensing

Background

During the past decades, many biosensors have been developed for more sensitive and selective detection of target materials under various conditions. Among these, electrochemical sensors have raised interest due to their simplicity, rapid detectability, and low cost together with high sensitivity [1]. Additionally, they provide direct, specific, and real-time detection of target materials [2–4].

One of the critical factors that determines the performance of electrochemical sensors is the electrode where the reactions occur. Conventional macro-electrodes cannot access micro- and nanoenvironments due to their size. The development of nanoscale electrodes allows for the detection of single biomolecules [5] and single cell secretions [6], measurement of local concentration profiles, and in vivo monitoring of neuro-chemical events [7]. Nanoelectrodes have other advantages regarding diffusion and size. Molecular analytes are consumed at an electrode surface as electrolysis

proceeds during an electrochemical redox reaction, making a concentration gradient for fresh analyte to diffuse from the bulk solution. At macroelectrodes, linear diffusion dominates, resulting in limited mass transport. On the other hand, radial diffusion dominates at nanoelectrodes with consequent enhanced rates of analyte mass transport to an electrode. Thus, nanoelectrodes can be used to study faster electrochemical and chemical reactions. In addition, size reduction of each electrode and increase in the total number of electrodes can improve the detection limits and the signal-to-noise (S/N) ratio because the noise level depends on the active area of the individual electrode while the signal depends on the total area of the electrodes [8].
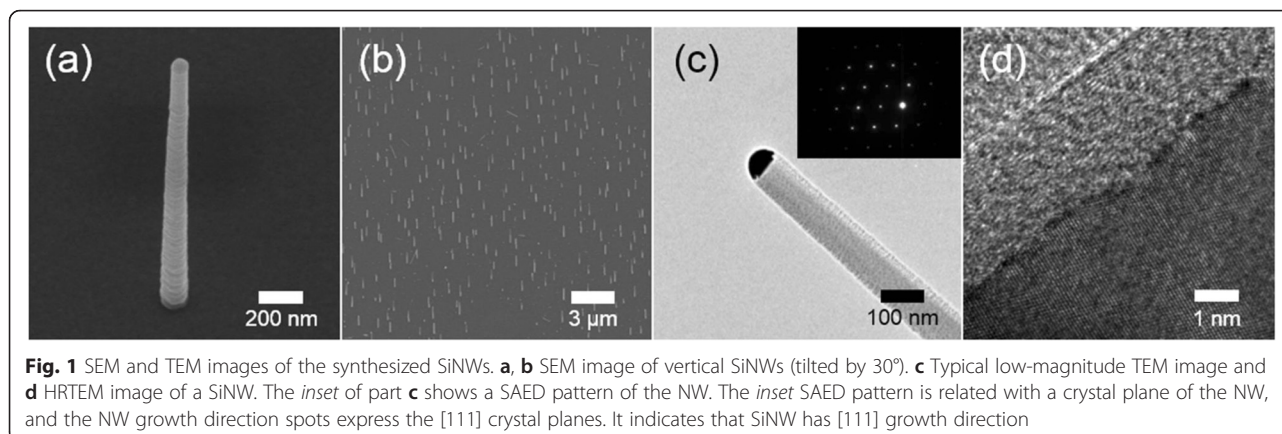
Several nanomaterials have been studied as electrodes including nanoparticles (NPs) [9, 10], nanobelts (NBs) [11, 12], nanorods (NRs) [13], and nanotubes (NTs) [14, 15]. Nanoparticles, commonly used for biosensors, show high sensitivity for detection, but their sensing properties often suffer from degradation as a result of the growth of aggregates among the nanoparticles when operated at high temperature for long times [16]. Moreover, difficulties in controlling the particle size deviation and uniform dispersion

* Correspondence: yblim@yonsei.ac.kr; hjc@yonsei.ac.kr
†Equal contributors
[1]Department of Materials Science and Engineering, Yonsei University, Seoul 03722, South Korea
Full list of author information is available at the end of the article

Lee *et al. Nanoscale Research Letters* (2016) 11:341

Page 2 of 7

Fig. 1 SEM and TEM images of the synthesized SiNWs. **a, b** SEM image of vertical SiNWs (tilted by 30°). **c** Typical low-magnitude TEM image and **d** HRTEM image of a SiNW. The *inset* of part **c** shows a SAED pattern of the NW. The *inset* SAED pattern is related with a crystal plane of the NW, and the NW growth direction spots express the [111] crystal planes. It indicates that SiNW has [111] growth direction

hinder the development and characterization of nano-integrated devices.

Nanowires (NWs), which can solve these problems, have advantages as building blocks for electrochemical sensors, such as relatively simple preparation methods allowing large-scale production, superior stability due to high crystallinity, and very large surface-to-volume (S/V) ratio. The latter are mandatory for fast reaction kinetics and high density loading of a target species and catalyst deposition over the surface for the induction or inhibition of specific reactions [16]. Thus, one-dimensional (1D) NWs are potential candidates for future sensors.

In this study, we propose an electrochemical biosensor by combining the NWs with artificial peptides designed to recognize HIV-1 Rev response element (RRE) RNA. Developing device aspects to enhance sensor properties, we also used artificial peptides instead of intact proteins. Artificial peptides are economic, easy to synthesize, and are small in size. Additionally, it is easy to change their properties by modifying the side chains. Using the advantages of both the NWs and artificial peptides, we demonstrate ultra-sensitive and -selective detection of HIV-1 RRE RNA.

Methods

Reagents and Materials

Rink amide MBHA resin LL and all Fmoc-protected amino acids were purchased from Novabiochem. Fmoc-Ebes-OH was purchased from Anaspec. N-Methyl-2-pyrrolidone was purchased from Merck. Other solvents were purchased from Sigma-Aldrich. Peptide was synthesized on Rink Amide MBHA resin LL using standard Fmoc protocols via a Tribute™ peptide synthesizer (Protein Technologies, Inc.). The peptides were purified by reverse-phase high-performance liquid chromatography (HPLC, water-acetonitrile with 0.1 % TFA). Concentration was determined spectrophotometrically using a molar extinction coefficient of TAMRA (80,400 M^{-1} cm^{-1}) at 547 nm.

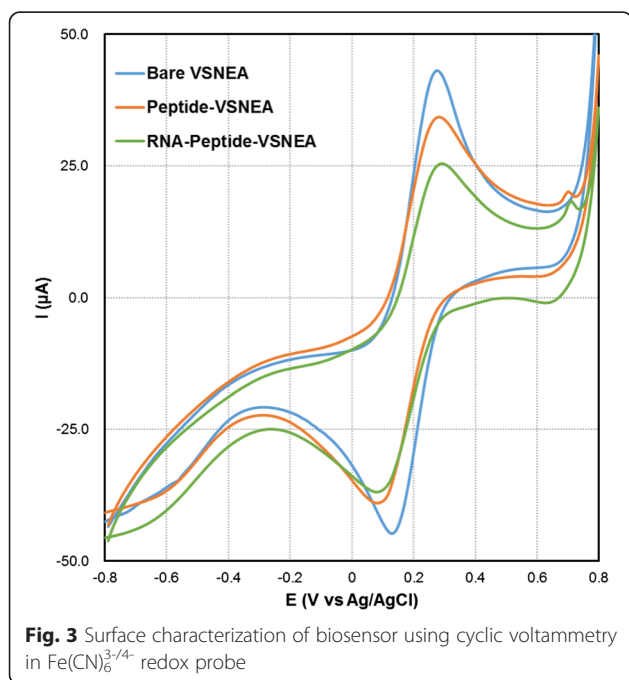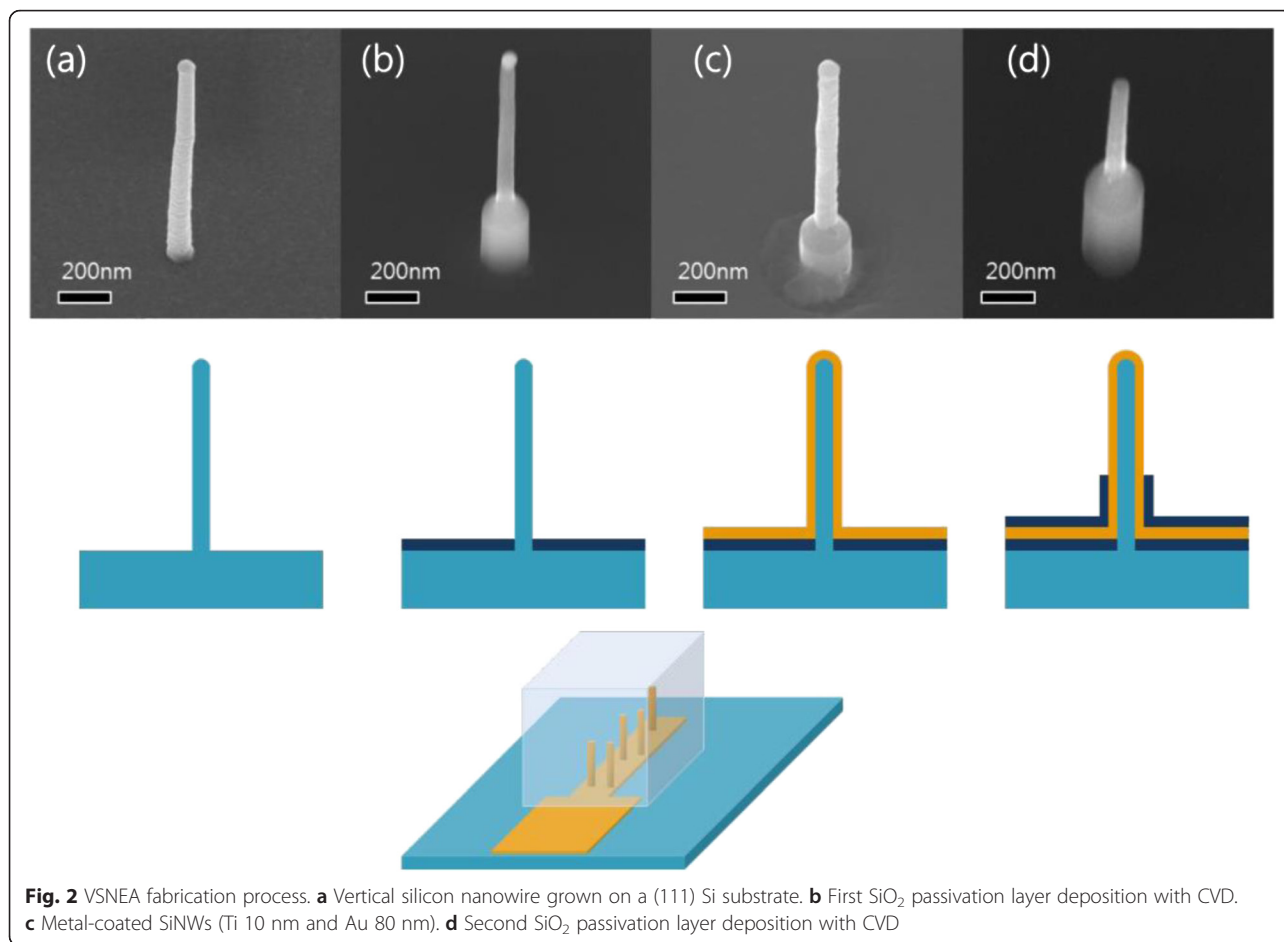### Growth of Silicon Nanowires and Fabrication of Electrodes

The Au-coated vertical silicon nanowire electrode array (VSNEA) was fabricated using the procedures described previously [17, 18] modified as follows. Si (111) substrate was deposited in 0.1 vol.% 3-aminopropyl triethoxysilane (APTES) solution in absolute ethanol. Au catalysts were then coated by immersing the substrate in the colloid solution having Au particles with 250-nm diameter. The substrate was placed in a chemical vapor deposition (CVD) reactor after washing and drying. Silicon nanowires (SiNWs) were vertically grown (with controlled diameter, length, and growth density) on the substrate by flowing $SiCl_4$ and H_2 gas. To fabricate the VSNEA, SiNWs were added a metal layer (Au = 80 nm and Ti = 10 nm) and a SiO_2 passivation layer onto the surface of the substrate using a sputtering process at a rate of 5 nm/min. Then, the SiO_2 passivation layer was selectively etched out to expose the Au tips at the top of the NWs by a complementary metal-oxide semiconductor (CMOS) process.

Peptide Immobilization and RNA Functionalization

The peptide immobilization on VSNEA was carried out by infusing 50 μL of 40 μM peptide in 25 °C environments. The peptide and Au-coated SiNWs were bound by covalent interaction using cysteine (C; this amino acid is expressed in the sequence of peptide in Fig. 4), which has sulfhydryl group, for stability of binding sites. After 12 h for peptide immobilization, RNA was injected to VSNEA using RNase-free water to functionalize with the peptide, and was further incubated for 12 h. Between every immobilization and functionalization step, the VSNEA was washed with distilled water to remove unattached biomolecules.

Electrochemical Analysis

The cyclic voltammetry (CV) and differential pulse voltammetry (DPV) measurements were performed with 20 mM potassium ferrycianide in 50 mM

Lee *et al. Nanoscale Research Letters* (2016) 11:341

Page 3 of 7

Fig. 2 VSNEA fabrication process. **a** Vertical silicon nanowire grown on a (111) Si substrate. **b** First SiO_2 passivation layer deposition with CVD. **c** Metal-coated SiNWs (Ti 10 nm and Au 80 nm). **d** Second SiO_2 passivation layer deposition with CVD

Fig. 3 Surface characterization of biosensor using cyclic voltammetry in $Fe(CN)_6^{3-/4-}$ redox probe
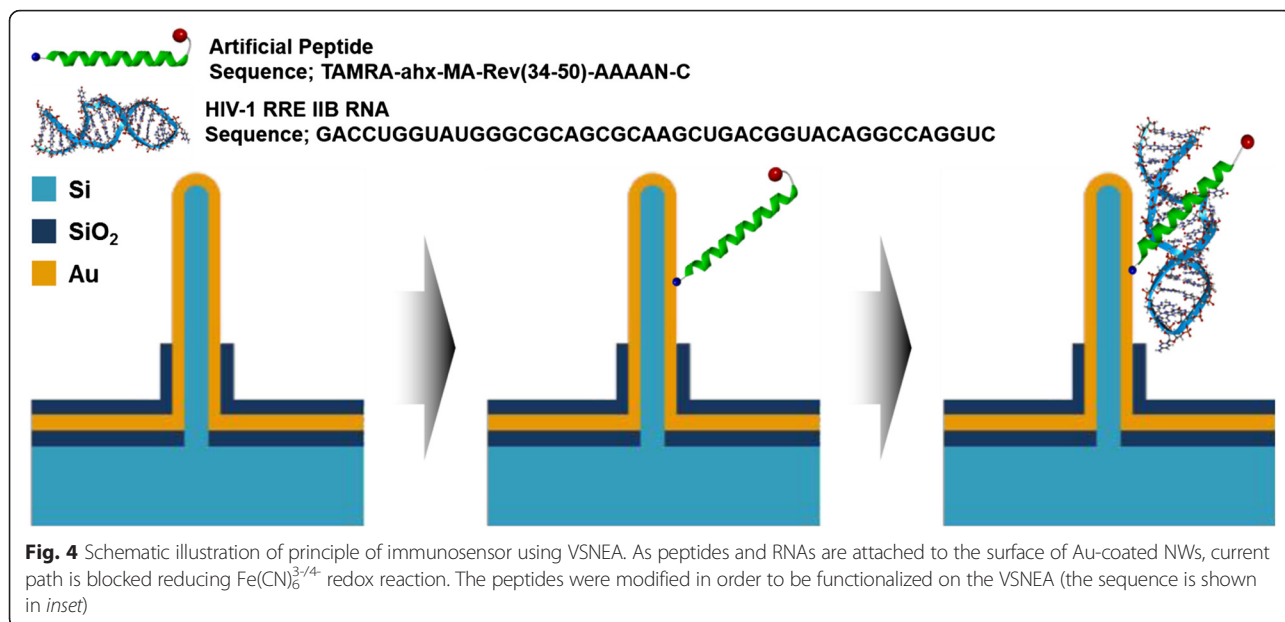
phosphate-buffered saline (PBS) solution. CV measurements were carried out in a potential range of 0.8 to −0.8 V and the scan rate was 20 mV/s. Sensitivity and selectivity were measured by DPV with a potential range from −0.2 to 0.6 V, pulse amplitude of 50 mV, and pulse width of 10 ms.

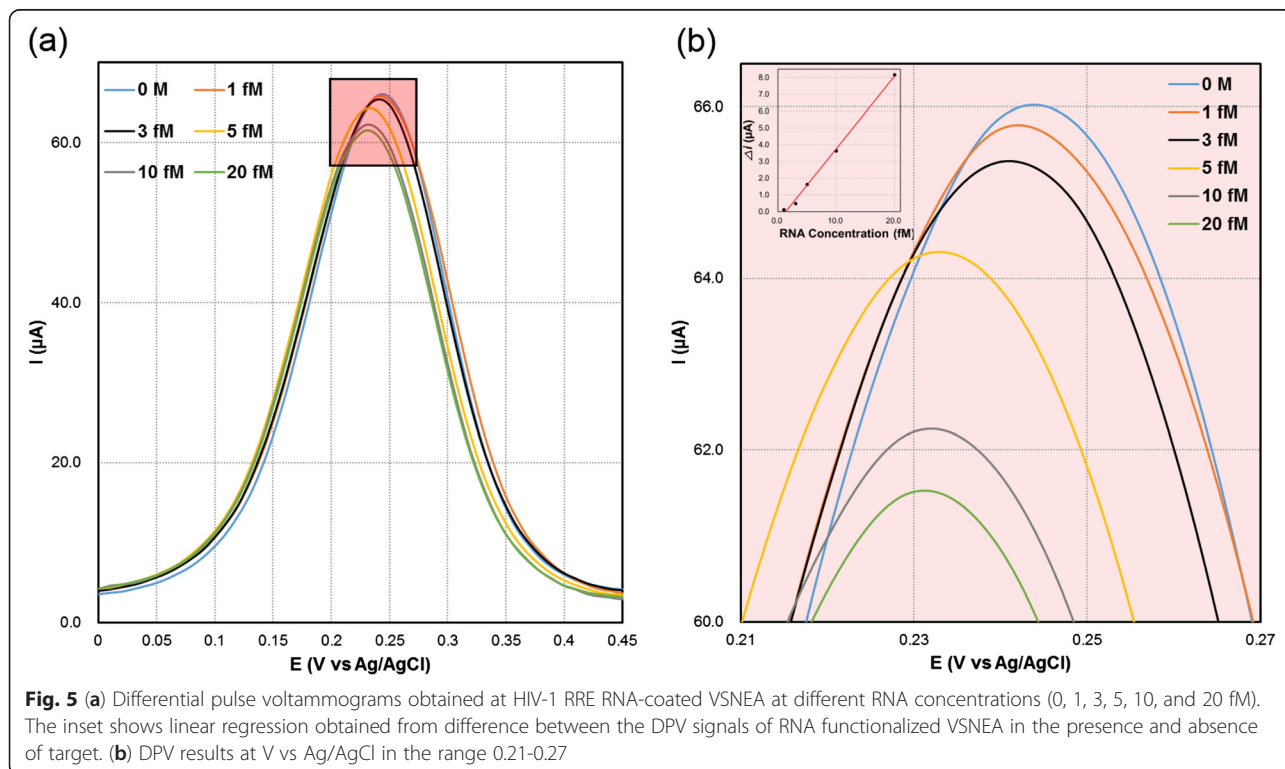## Results and Discussion

Growth of SiNWs and Fabrication of Electrodes

Figure 1a, b shows scanning electron microscopy (SEM) images of the SiNWs vertically grown on the substrate. The length of the SiNWs is approximately 3 μm. Figure 1c shows a metal globule at the tip of a NW that indicates the working of the vapor-liquid-solid (VLS) mechanism for the growth of SiNWs. The inset in Fig. 1c shows the selected area electron diffraction (SAED) pattern showing that the SiNWs are single-crystalline and grow along the [111] direction. The diameter of the SiNWs was approximately 200 nm. The single-crystalline nature with a thin native oxide layer and a thickness of about 3 nm is also observed in a high-resolution transmission electron microscopy (HRTEM) image (Fig. 1d).

Lee *et al. Nanoscale Research Letters* (2016) 11:341

Page 4 of 7

Fig. 4 Schematic illustration of principle of immunosensor using VSNEA. As peptides and RNAs are attached to the surface of Au-coated NWs, current path is blocked reducing $Fe(CN)_6^{3-/4-}$ redox reaction. The peptides were modified in order to be functionalized on the VSNEA (the sequence is shown in *inset*)

The diameter and length of the SiNWs could be controlled by the size of Au colloidal particles and growth time. The density of SiNWs on the substrate could also be controlled by the concentration of Au nanoparticles in the colloidal solution. Previous studies have shown that the density and size of NWs that are electrodes of a device can change the properties like sensitivity and selectivity of the NW-based sensors [19].

As mentioned in the introduction, size reduction of each electrode and increase in the total number of electrodes can improve the detection limits and the S/N ratio since the noise level depends on the active area of the individual electrode whereas the signal depends on the total area of the electrodes [8]. In this research, the VSNEA behaves as an electrode with a partially blocked surface operating under total overlap diffusion conditions [20]. Therefore, if
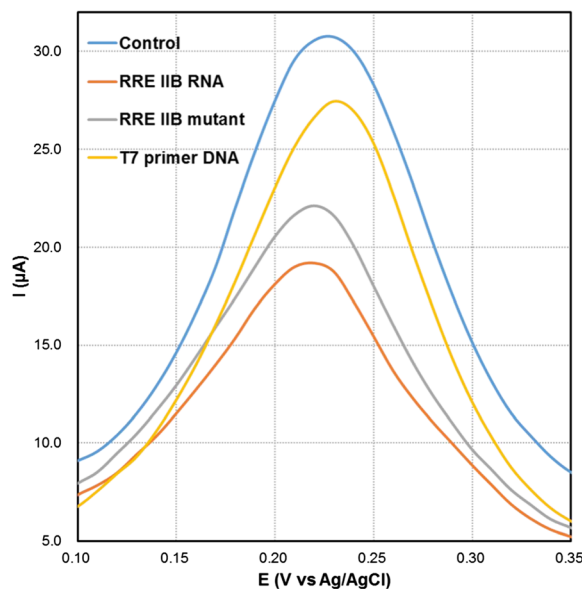

Fig. 5 (**a**) Differential pulse voltammograms obtained at HIV-1 RRE RNA-coated VSNEA at different RNA concentrations (0, 1, 3, 5, 10, and 20 fM). The inset shows linear regression obtained from difference between the DPV signals of RNA functionalized VSNEA in the presence and absence of target. (**b**) DPV results at V vs Ag/AgCl in the range 0.21–0.27

Lee *et al. Nanoscale Research Letters* (2016) 11:341

Page 5 of 7

Fig. 6 Differential pulse voltammograms of Fe(CN)$_6^{3-/4-}$ at blank (peptide-coated), RNA-coated VSNEA, RNA mutant-coated VSNEA, and DNA-coated VSNEA

we consider voltammetric experiment peak current (the signal, S) and capacitive currents (the main component of the noise, N) at the VSNEA under a total overlap regime, then we obtain the following equations [19].

$$S = I_p = 2.69 \times 10^5 \frac{3}{n^2} A_{geom} v^{\frac{1}{2}} D^{\frac{1}{2}} C_b \qquad (1)$$

$$N = I_c = A_{act} C_d \qquad (2)$$

$(A_{act} = active\ area, A_{geom} = $ total geometrica area,
$v = $ scan rate, $D = $ diffusion coefficient, $C = $ concentration$)$

Here, the active area, A_{act}, is the area of the Au-coated, non-passivated surface of nanowires exposed to the medium and the geometric area and A_{geom}, is the total area including the active area and all the passivated surfaces of nanowires and substrates. At conventional electrode, in the same experimental conditions, Eqs. (3) and (4) are given.

$$S = I_p = 2.69 \times 10^5 \frac{3}{n^2} A_{geom} v^{\frac{1}{2}} D^{\frac{1}{2}} C_b \qquad (3)$$

$$N = I_c = A_{geom} C_d \qquad (4)$$

Combining equations from Eqs. (1, 2, 3, and 4) gives Eq. (5).

$$\left(\frac{S}{N}\right) NEA = \left(\frac{S}{N}\right) CONV \times \frac{A_{geom}}{A_{act}} \qquad (5)$$

(NEA; nano electrode array, CONV; conventional electrode).

Equation (5) shows that the S/N ratio of the NEA is higher than that at a conventional electrode because A_{geom}/A_{act} values are generally below 10^{-3} [21]. This means that detection limits of such devices are two to three orders of magnitude better than that of conventional macroelectrodes [22]. The reaction rate can further be enhanced in the nanowire electrodes since a vertically aligned nanowire can work as an "electron antennae" and enhance the electron transfer for the reactions [23, 24].

Figure 2 shows the scheme of Au-coated VSNEA fabrication using vertical SiNWs. Figure 2a shows the SiNWs grown vertically on the substrate. SiNWs were then covered with SiO$_2$ passivation layer through a CVD process and then selectively etched to expose the SiNWs (Fig. 2b). Polymethyl methacrylate resists serving as a SiO$_2$ protecting layer was coated on the substrate, and buffered oxide etch was used to selectively etch the SiO$_2$ layer on the NWs. Au film was then deposited on the surface of SiNWs to immobilize the peptides (Fig. 2c). Finally, the substrate was coated with a secondary SiO$_2$ passivation layer and then selectively etched to expose the Au layer only at the tip of VSNEA (Fig. 2d).

Immobilization of RNA onto VSNEA

The VSNEA in this study was combined with artificial peptides to recognize the HIV-1 RRE. The immobilization of peptides on the surface of VSNEA was investigated by CV measurement. Figure 3 shows CV under bare and immobilized conditions. We use a wide potential scan range to investigate the way of working of this kind of electrodes as well as get the information of electrochemical reactions.

The bare VSNEA produces well-defined redox peaks with a cathodic peak potential (E_{pc}) of 0.28 mV and an anodic peak potential (E_{pa}) of 0.13 mV in the potential range of 0.8 to −0.8 V with 43.05 μA of anodic peak current (I_a). These peaks are attributed to the redox reaction at the VSNEA surface. The anodic peak current decreases gradually as the peptide (34.32 μA) and the RNA (25.46 μA) were immobilized on the surface of VSNEA. This happens because the peptides and RNA cover the VSNEA surface and interrupt ion transfer with blocking current pathway (Fig. 4). These immobilization and functionalization reduce redox reaction ($Fe(CN_6)^{4-} \leftrightarrow Fe(CN_6)^{3-} + e$) inducing peak current decrease. The CV measurements thus confirmed the immobilization of the peptides on the surface of the VSNEA.

Detection of Different Concentrations of RNA

The efficiency of VSNEA as a biosensor is explored by detection of RRE IIB RNA. The detection was carried out via DPV, which is a highly sensitive analytical method used for the quantitative determination of analytes. Figure 5 shows DPV signals of RNA functionalized VSNEA which exhibit (a) 65.83, (b) 65.71, (c) 65.34, (d) 64.20, (e) 62.19, and (f) 61.49 μA as the concentration of RRE IIB RNA changes from 1 to 20 fM. This clearly shows that the peak current was proportional to the RNA concentration.

The inset of Fig. 5 depicts the linear correlation of the differences in peak currents, [$I_p(c) = I_p \ (c = 0) - I_p \ (c)$] with respect to the target RNA concentration. The regression equation for the peak current (I), and the concentration of the target RNA (c), shows a correlation coefficient (R^2) of 0.99557 with standard deviation of $\pm 2.3 10^{-7}$ fM. Detection limit was calculated to be 1.513 fM. Recent HIV-1 biosensors using nanomaterials such as nanopore [25], nanoparticle [26], and graphene composite film [27] showed detection limits from tens of fM to nM. Compared to these, the detection limits of VSNEA in this study show superior detectability. This is due to the nanosize and unique shape of nanowire as an electrode, which cause enhanced mass transport and fast electron-transfer kinetics [28, 29]. In addition, total overlap diffusion with proper electrode structure, size, and distance between the electrode elements make it possible to achieve very high sensitivity with fM detection limit.

Detection of Mutated RNA

The working of VSNEA as a biosensor is also explored by the detection of different types of RRE IIB. Three different types [RRE IIB RNA (complementary), RRE IIB mutant and T7 primer DNA] were evaluated by DPV measurement. The sequences used were as follows:

RRE IIB RNA sequence:

GACCUGGUAU**G**GGCGCAGCGCAAGCUGACGG UA**C**AGGCCAGGUC

RRE IIB mutant sequence:

GACCUGGUAU**C**GGCGCAGCGCAAGCUGACGGU A**G**AGGCCAGGUC

T7 primer DNA sequence: TAATACGACTCACTATA GGAG

Figure 6 shows DPV responses for the mutated RNA. The bare RRE IIB RNA shows the highest DPV response followed by the RRE IIB mutant and the T7 primer DNA. This is because the Rev peptide specifically binds to RRE IIB wild type and the C46-G74 mutation reduces affinity of the Rev peptide. The well-structured RRE RNA provides space for Rev proteins to bind specifically via interactions such as hydrogen bonds. Base-pair mutations of RNA result in changes of the binding space. DNA provides a completely different space compared with RRE RNA, and there is only an electrostatic interaction between the negatively charged DNA and the positively charged peptide. Therefore, it is harder for Rev proteins to bind DNA or mutant RRE than RRE RNA and these differences of binding interaction induced a DPV peak current change between the blank (30.72 μA) and the T7 primer DNA (27.45 μA), RRE IIB mutant (22.11 μA), and RRE IIB RNA (19.18 μA). Compared to RRE IIB RNA, these two types showed noticeable difference and demonstrate that the electrochemical biosensor based on VSNEA is effective in signaling the presence of a complementary target and discriminating targets from a single base-pair substitution mutation.

Conclusions

Sensitive and selective detection of HIV-1 RNA by using VSNEA combined with artificial peptides was demonstrated. The advantages of vertical, 1D nanowire electrodes such as high surface area to volume ratio and total overlap diffusion of ions make it possible to detect RNA concentrations of up to 1.513 fM and distinguish between wild-type RNA and mutant RNA. Thus, vertical nanowire sensors may be used as sensitive and selective biosensor platforms in many applications.

Authors' contributions
JL and MHH carried out the experiment and drafted the manuscript. SH participated in the biomolecule synthesis. JN, IK, YJK, YbL, and HJC participated in the design of the study and drafted the manuscript. All authors read and approved the final manuscript.

Competing interests
The authors declare that they have no competing interests.

Lee *et al. Nanoscale Research Letters* (2016) 11:341

Page 7 of 7

Author details
[1]Department of Materials Science and Engineering, Yonsei University, Seoul 03722, South Korea. [2]Defense Advanced R&D Center, Agency for Defense Development, Daejeon 34186, South Korea.

References
1. Munde M, Ismail MA, Arafa R, Peixoto P, Collar CJ, Liu Y, Hu L, David-Cordonnier MH, Lansiaux A, Bailly C, Boykin DW, Wilson WD (2007) Design of DNA minor groove binding diamidines that recognize GC base pair sequences: a dimeric-hinge interaction motif. J Am Chem Soc 129:13732–13743
2. Wanekaya AK, Chen W, Myung NV, Mulchandani A (2006) Nanowire-based electrochemical biosensors. Electroanalysis 18:533–550
3. Wang J (2006) Electrochemical biosensors: towards point-of-care cancer diagnostics. Biosens Bioelectron 21:1887–1892
4. Feigel IM, Vedala H, Star A (2011) Biosensors based on one-dimensional nanostructures. J Mater Chem 21:8940–8954
5. Fan FRF, Kwak J, Bard AJ (1996) Single molecule electrochemistry. J Am Chem Soc 118:9669–9675
6. Amatore C, Arbault S, Guille M, Lemaitre F (2008) Electrochemical monitoring of single cell secretion: vesicular exocytosis and oxidative stress. Chem Rev 108:2585–2621
7. Kennedy RT, Huang L, Atkinson MA, Dush P (1993) Amperometric monitoring of chemical secretions from individual pancreatic beta-cells. Anal Chem 65:1882–1887
8. Tu Y, Lin YH, Ren ZF (2003) Nanoelectrode arrays based on low site density aligned carbon nanotubes. Nano Lett 3:107–109
9. De M, Ghosh PS, Rotello VM (2008) Applications of nanoparticles in biology. Adv Mater 20:4225–4241
10. Ansari SG, Boroojerdian P, Sainkar SR, Karekar RN, Aiyer RC, Kulkarni SK (1997) Grain size effects on H-2 gas sensitivity of thick film resistor using SnO2 nanoparticles. Thin Solid Films 295:271–276
11. Chen X, Zou G, Deng Y, Zhang Q (2008) Synthesis and nonlinear optical properties of nanometer-size silver-coated polydiacetylene composite vesicles. Nanotechnology 19:195703
12. Comini E, Faglia G, Sberveglieri G, Pan ZW, Wang ZL (2002) Stable and highly sensitive gas sensors based on semiconducting oxide nanobelts. Appl Phys Lett 81:1869–1871
13. Chen YJ, Nie L, Xue XY, Wang YG, Wang TH (2006) Linear ethanol sensing of SnO2 nanorods with extremely high sensitivity. Appl Phys Lett 88:083105
14. Patzke GR, Krumeich F, Nesper R (2002) Oxidic nanotubes and nanorods—anisotropic modules for a future nanotechnology. Angew Chem Int Ed Engl 41:2446–2461
15. Bae C, Yoo H, Kim S, Lee K, Kim J, Sung MA, Shin H (2008) Template-directed synthesis of oxide nanotubes: fabrication, characterization, and applications. Chem Mater 20:756–767
16. Ramgir NS, Yang Y, Zacharias M (2010) Nanowire-based sensors. Small 6:1705–1722
17. Kim I, Kim SE, Han S, Kim H, Lee J, Jeong DW, Kim JJ, Lim YB, Choi HJ (2013) Large current difference in Au-coated vertical silicon nanowire electrode array with functionalization of peptides. Nanoscale Res Lett 8:502
18. Kim I, Lee HY, Kim H, Lee E, Jeong DW, Kim JJ, Park SH, Ha Y, Na J, Chae Y, Yi S, Choi HJ (2015) Enhanced neurite outgrowth by intracellular stimulation. Nano Lett 15:5414–5419
19. Ugo P, Moretto LM, Vezza F (2002) Ionomer-coated electrodes and nanoelectrode ensembles as electrochemical environmental sensors: recent advances and prospects. Chemphyschem 3:917–925
20. De Leo M, Kuhn A, Ugo P (2007) 3D-ensembles of gold nanowires: preparation, characterization and electroanalytical peculiarities. Electroanalysis 19:227–236
21. Menon VP, Martin CR (1995) Fabrication and evaluation of nanoelectrode ensembles. Anal Chem 67:1920–1928
22. Ugo P, Moretto LM, Bellomi S, Menon VP, Martin CR (1996) Ion-exchange voltammetry at polymer film-coated nanoelectrode ensembles. Anal Chem 68:4160–4165
23. Zhao W, Sun SX, Xu JJ, Chen HY, Cao XJ, Guan XH (2008) Electrochemical identification of the property of peripheral nerve fiber based on a biocompatible polymer film via in situ incorporating gold nanoparticles. Anal Chem 80:3769–3776
24. Ramulu TS, Venu R, Sinha B, Lim B, Jeon SJ, Yoon SS, Kim CG (2013) Nanowires array modified electrode for enhanced electrochemical detection of nucleic acid. Biosens Bioelectron 40:258–264
25. Wang L, Han YJ, Zhou S, Guan XY (2014) Real-time label-free measurement of HIV-1 protease activity by nanopore analysis. Biosens Bioelectron 62:158–162
26. Liu JK, Du BC, Zhang PH, Haleyurgirisetty M, Zhao J, Ragupathy V, Lee S, Devoe DL, Hewlett IK (2014) Development of a microchip Europium nanoparticle immunoassay for sensitive point-of-care HIV detection. Biosens Bioelectron 61:177–183
27. Li B, Li ZL, Situ B, Dai Z, Liu QL, Wang Q, Gu DY, Zheng L (2014) Sensitive HIV-1 detection in a homogeneous solution based on an electrochemical molecular beacon coupled with a nafion-graphene composite film modified screen-printed carbon electrode. Biosens Bioelectron 52:330–336
28. Lin YH, Lu F, Tu Y, Ren ZF (2004) Glucose biosensors based on carbon nanotube nanoelectrode ensembles. Nano Lett 4:191–195
29. Hoeben FJM, Meijer FS, Dekker C, Albracht SPJ, Heering HA, Lemay SG (2008) Toward single-enzyme molecule electrochemistry: [NiFe]-hydrogenase protein film voltammetry at nanoelectrodes. ACS Nano 2:2497–2504